# Sharp variation in coercivity and magnetic interactions in patterned CoxNi1x nanoarrays

Chao-Yao Yang, Liang-Wei Wang, Po-An Chen, Hong-Ji Lin, Chih-Huang Lai, and Yuan-Chieh Tseng

Citation: Journal of Applied Physics **114**, 063902 (2013); doi: 10.1063/1.4817866
View online: http://dx.doi.org/10.1063/1.4817866
View Table of Contents: http://scitation.aip.org/content/aip/journal/jap/114/6?ver=pdfcov
Published by the AIP Publishing

# Sharp variation in coercivity and magnetic interactions in patterned $Co_xNi_{1-x}$ nanoarrays

Chao-Yao Yang,[1] Liang-Wei Wang,[2] Po-An Chen,[1] Hong-Ji Lin,[3] Chih-Huang Lai,[2] and Yuan-Chieh Tseng[1,a)]

[1]*Department of Materials Science & Engineering, National Chiao Tung University, 1001 Ta Hsueh Road, Hsinchu 30010, Taiwan*

[2]*Department of Materials Science and Engineering, National Tsing Hua University, Hsinchu 30043, Taiwan*

[3]*National Synchrotron Radiation Research Center, Taiwan, 101 Hsin Ann Road, Hsinchu Science Park, Hsinchu 30076, Taiwan*

(Received 21 May 2013; accepted 24 July 2013; published online 8 August 2013)

We present a study concerning the unexpectedly large coercivity increase and associated magneto-structural properties of $Co_xNi_{1-x}$ patterned arrays. An increase in $x$ led to an face-center-cubic (FCC)→hexagonal-close-packed (HCP) transition in $Co_xNi_{1-x}$ arrays, accompanied by a 6-fold increase in coercivity and strong 3*d* exchange interactions probed by x-ray magnetic circular dichroism. Sum-rule analysis revealed that orbital moment involved very little in the variable coercivity and magnetic anisotropy; this is distinct from other nanostructures displaying variable coercivity. The sharp rise in coercivity can be attributed to the geometrical confinement of the arrays, causing the microstructure of the nano-clusters to switch magnetization reversal mechanism from fanning to coherent with increasing $x$, based on the chain-of-spheres model. First-order-reversal curves revealed that the FCC and HCP arrays comprised both soft and hard ferromagnetic components; however, the soft component of the FCC was much more pronounced, leading to differences in reversibility. This type of nanostructure provides a sharp control of magnetic hardness that could be tailored in related technologies. © *2013 AIP Publishing LLC*.
[http://dx.doi.org/10.1063/1.4817866]

The ultra-high packing density of patterned ferromagnetic (FM) media[1–4] may one day replace current thin film media in the next generation of magnetic storage. Bimetallic, nano-array media exhibit interesting phenomena resulting from high structural confinement and physical proximity effects. Co has long been a central component of recording media,[5,6] due to its ability to produce strong perpendicular magnetic anisotropy (PMA) when alloyed with Pt and Pd.[7–9] The magneto-structural interaction of Co with the other elements determines the properties of the resulting media; however, this topic remains poorly understood with regard to patterned media. This study examined the $x$-dependent structural and magnetic evolutions of $Co_xNi_{1-x}$ nano-arrays. Compared to CoPt/CoPd, CoNi is more economical, non-toxic, and not compositionally limited by the $L1_0$ phase. In addition, the high-order arrays and various techniques employed in this study provide a unique setting to investigate the fundamental physics underlying patterned media. We examined coupled reversal-dynamics and microstructural properties as well as the modification of macro- and micro-magnetism across the structural transition. Our results indicate that the structural geometry and microstructure of the arrays greatly improved the hardness of the media as the concentration entered the hexagonal-close-packed (HCP) region. This provided a simple strategy by which to alleviate Co-based alloys (except CoPt/CoPt) from low coercivity when formed into nanostructures.

This study fabricated $Co_xNi_{1-x}$ nano-arrays using electroless plating with porous anodic alumina oxide (AAO). The plating technique and experimental process are detailed in our previous studies.[4,10] Five samples with $x = 10$, 30, 50, 70, and 90 at. % were prepared and labeled as CN10, CN30, CN50, CN70, and CN90, respectively. The morphologies and microstructures of the arrays were probed using scanning electronic microscopy and transmission electronic microscopy, respectively. Crystallographic properties were characterized using Cu kα x-ray diffraction (XRD). Magnetic hysteresis (M-H) loops were measured along the long axis of the arrays using a vibrating sample magnetometer (VSM). X-ray magnetic circular dichroism (XMCD) spectra were acquired in total electron yield mode, operated over Co/Ni $L_2$ and $L_3$ absorption edges. We then employed sum-rule analysis[11] to obtain the spin ($S_z$) and orbital ($L_z$) atomic moments. First-order reversal curve (FORC) diagrams[12–14] were also collected using a VSM below (CN50) and above (CN90) the structural transition. We selected CN50 instead of CN10 to represent the face-center-cubic (FCC) group because the larger $H_c$ of CN50 is capable of providing better resolution with regard to FORC distribution. Following saturation, we measured magnetization starting from a reversal field, defined as $H_r$, back to the positive saturation to trace out a FORC. A family of FORCs was obtained with different $H_r$ but equal field spacing filling the interior of the major hysteresis loop. Finally, FORC diagrams were presented in a contour plot by mathematically converting the coordination from $H_r/H_a$ ($H_a$ is applied field) into $H_b/H_c$, according to the following equations: $H_c = (H_a - H_r)/2$ and $H_b = (H_a + H_r)/2$.

a)Author to whom correspondence should be addressed: Electronic mail: yctseng21@mail.nctu.edu.tw

 

Each FORC family contained 150 FORC measurements. The FORC saturation fields were 5200 and 9100 Oe for CN50 and CN90, respectively, and their $H_a$ and $H_r$ field intervals were both 71 Oe. Details regarding FORC analysis can be found in Refs. 12–14.

Figures 1(a) and 1(b), respectively, present cross-sectional and top-view SEM images of the $Co_xNi_{1-x}$ nano-arrays, enabling the acquisition of the free-standing and isolated natures of the arrays on a Si substrate with an aspect ratio of approximately 3. All $Co_xNi_{1-x}$ samples exhibited identical dimensions, due to the confinement of the AAO template. The microstructure probed by TEM is presented in Fig. 1(c) in which CN50 was selected to illustrate the cluster microstructure of the arrays with cluster-units ~30 nm in diameter. The microstructure of the clusters can be attributed to the manner in which the EL-plated nano-arrays were grown.[10] Similar micrographs were found in other investigated samples (data not provided). Figure 2(a) presents the *x*-dependent crystallographic properties of the $Co_xNi_{1-x}$ probed by XRD. A Ni-based, FCC structure was obtained in CN10, CN30, and CN50 with (111) and (200) indices, while an HCP structure was acquired in CN70 and CN90 with (002) index due to the dominance of a Co-rich phase. An FCC→HCP structural transition occurred between CN50 and CN70. The transition was fairly sharp, with no mixed-phase obtained in CN50. The composition obtained for the structural transition is consistent with bulk CoNi,[15] suggesting that the $Co_xNi_{1-x}$ possesses high structural stability when formed in patterned arrays. Figure 2(b) presents *x*-dependent M-H curves, with the saturation magnetization ($M_s$) enhanced linearly with increasing *x*, due to larger 3*d* moments of Co than Ni, as predicted by the Slater-Pauling curve.[16] A large discontinuity in coercivity ($H_c$) accompanied the FCC→HCP structural transition, increasing from ~300 to ~1800 Oe as detailed in the inset of Fig. 2(b). The vast change in $H_c$ appears to have arisen from the varying degrees of magneto-crystalline anisotropy (MCA) accompanying the structural transition. However, CN70 and CN90 displayed an $H_c$ of ~1800 Oe, a value much greater than those of HCP-CoNi nanoparticles[17,18] with comparable dimensions. This implies that the variability of MCA is not necessarily the sole mechanism involved in the enormous increase in $H_c$.

Figure 3(a) provides *x*-dependent XMCD spectra for Co (left) and Ni (right). Interestingly, both Co and Ni XMCD

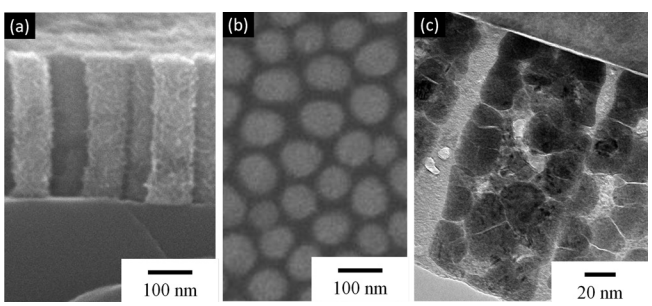


FIG. 1. (a) Cross-sectional and (b) top-viewed SEM images of CN50 as a representative for the appearance of EL $Co_xNi_{1-x}$ nano-arrays. The aspect ratio is about 3 for each rod featuring 100 nm in diameter and 300 nm in height. (c) TEM bright field image of CN50 arrays, showing a cluster-like microstructure. Each cluster is about 30 nm in diameter.

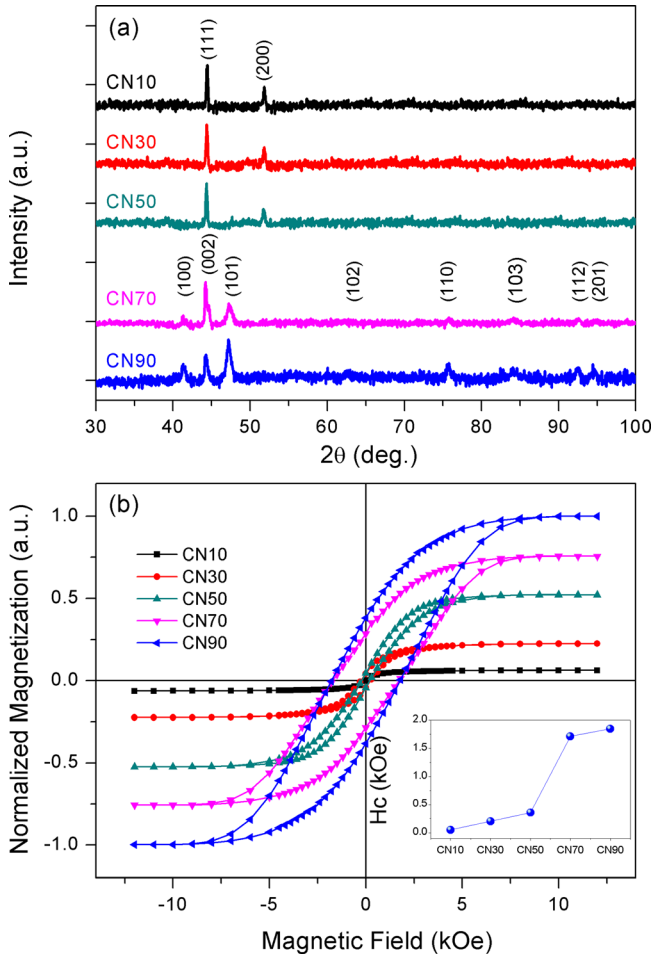


FIG. 2. (a) XRD patterns of $Co_xNi_{1-x}$ arrays with *x*-dependency. The FCC (CN10, CN30, and CN50) and HCP (CN70 and CN90) groups are crystallographically indexed. (b) *x*-dependent M-H curves of the $Co_xNi_{1-x}$ arrays, where all the magnetizations are normalized by that of CN90 for a better comparison. Insect of (b) shows *x*-dependent $H_c$ of $Co_xNi_{1-x}$ arrays, with a discontinuity appearing between CN50 and CN70.

varied with *x*, suggesting that the atomic moments of two elements fluctuated as a result of compositional change. This is not expected according to Slater-Pauling theory, with its foundation in the interpretation of changes in the magnetization of bimetallic transition-metal alloys as a reflection of the total sum of 3*d* magnetic valence (MV);[16] i.e., the change in magnetization depends only on the varying fractions of both MV-rich and MV-poor elements, which in this study, are Co and Ni, respectively. Nonetheless, our results point to the strong sensitivity of magnetization associated with the interactions between MV-rich and MV-poor elements. Insets in Fig. 3(a) present detailed results about *x*-dependent $S_z$ (left inset) and $L_z$ (right inset). In this case, $S_z$ is one order of magnitude greater than $L_z$ for both elements, suggesting that the macroscopic magnetization is dominated by the former, which is in agreement with the situation observed in transition metals.[10,11] $S_z$ exhibited a linear *x*-dependency; however, a break-point was observed in $L_z$ between CN50 and CN70, for both elements. Because $S_z$ is much greater than $L_z$ and the trends of $S_z$ are coherent for Co and Ni, the increase in $S_z$ appears to be responsible for the linear increase in the magnetization of $Co_xNi_{1-x}$. This suggests that the enhancement of $M_s$ with increasing *x* was due to the increase in the

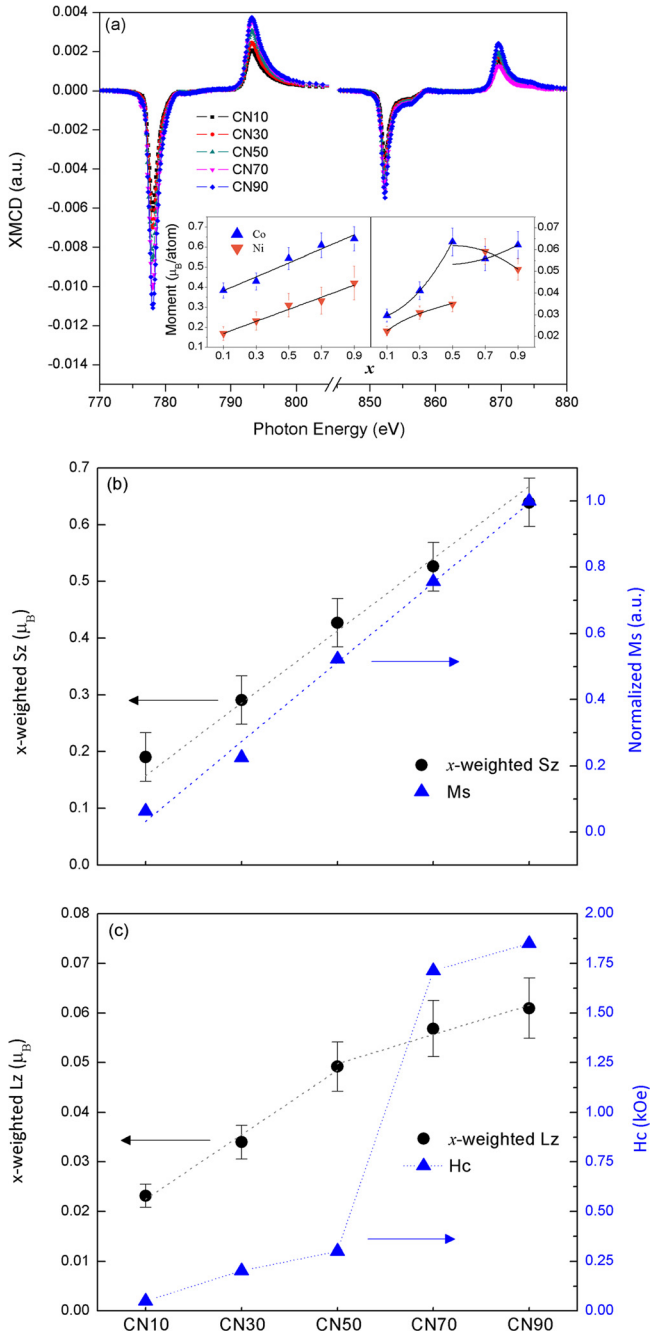


FIG. 3. (a) XMCD spectra for Co and Ni $L_2/L_3$ edges with $x$-dependency. All the XMCD signals are normalized by the corresponding XAS integrations. Insets are the sum-rule analyses of spin moment ($S_z$) (left) and orbital moment ($L_z$) (right) for Co (blue) and Ni (orange), respectively, with $x$-dependency. (b) Concentration-weighted $S_z$ (units on left y-axis) superimposed to normalized $M_s$ (units on right y-axis), with $x$-dependency. (c) Concentration-weighted $L_z$ (units on left y-axis) superimposed to $H_c$ (units on right y-axis), with $x$-dependency.

$S_z$ of both elements through $3d$ exchange interactions, instead of an increase in the fraction of MV.

$L_z$ is far more sensitive than $S_z$ to the structural transition of both elements. Unlike $S_z$, which can freely switch upon field reversal, $L_z$ is often bound to lattice and structural coordination, thereby serving as the origin of the MCA.[19–23] In fact, the promotion of $L_z$ is widely considered an effective strategy to improve spin-orbit coupling as a means to stabilize the magnetic state. Previous studies have revealed direct correlations between enhancements in $L_z$ and increases in the anisotropy constant[20,21] and $H_c$;[22,23] however, the correlations are mostly qualitative in scope. This fact motivated us to validate whether $L_z$ is responsible, especially quantitatively, for the enormous increase in $H_c$ within specific nanostructures. This study superimposed concentration-weighted $S_z$ and normalized $M_s$ in Fig. 3(b), and superimposed concentration-weighted $L_z$ and $H_c$ in Fig. 3(c), as a function of $x$. $S_z$ coincides well with $M_s$, indicating high correspondence between the two quantities. $L_z$, by contrast, shows a two-step increment which does not fully correspond to the sharp rise in $H_c$ across the transition. Quantitatively, $L_z$ increased only 20% from below (CN50) to above the transition (CN70), which is far below the 600% increase of $H_c$. Obviously, there must exist extrinsic factors governing the coercive responses of the arrays more effectively than $L_z$, despite a strong MCA provided by the HCP phase.

The low dimensional frameworks of magnetic nanostructures could confine the FM domain size and constrain the domain reversal, thereby influencing $H_c$. This study discovered that the microstructure of $Co_xNi_{1-x}$ arrays comprise many nano-clusters, the geometry of which reasonably fits a "chain-of-spheres (COS)" model.[24] In the COS model, single-domain (SD) particles are assumed to be linked within a chain structure. This geometry could produce two moment reversal mechanisms with different coercive responses, coherent and fanning reversal, as illustrated by the upper and lower schemes, respectively in Fig. 4. Coherent reversal often yields a larger $H_c$ than fanning because a larger magnetostatic energy barrier must be overcome through coherent switching. From TEM (Fig. 1(c)), we estimated the cluster size at 30 nm, a value smaller than the theoretical critical size (~100 nm) that favors the formation of SD within a particle.[19] Several researchers have reported that the critical size of SD particles in $Co_xNi_{1-x}$ nanostructures is approximately 40~60 nm.[25–28] Summarizing the above information,

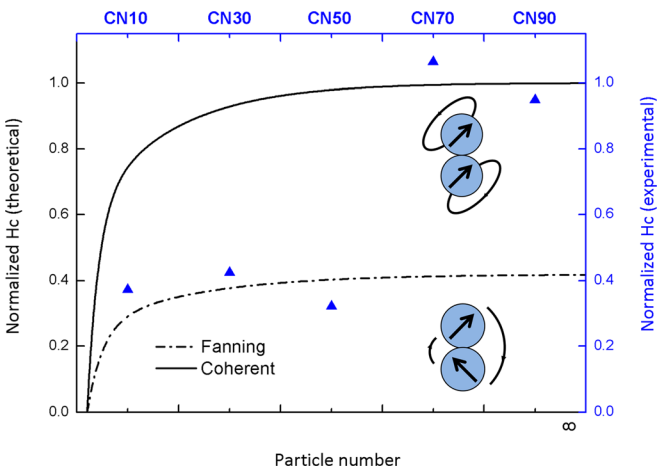


FIG. 4. Theoretical RI $H_c$ fitting for the $Co_xNi_{1-x}$ arrays using a COS model,[24] where the solid and dashed lines correspond to coherent and fanning reversals, respectively. The two reversal mechanisms are schematically illustrated under the corresponding lines. The fitting results count the particle number to infinity, and the results need to be interpreted by left and bottom axes with black color. In a similar fashion, normalized $H_c$ of the $Co_xNi_{1-x}$ arrays with $x$-dependency is superimposed to this figure as denoted by blue triangles, and the data need to be interpreted by right and upper axes with blue color.

we posit that it is reasonable to assign the COS model to this case in order to explain the coercive responses of $Co_xNi_{1-x}$.

This study used the COS model[19,24] to present theoretical $H_c$ as a function of particle number within a chain structure, for coherent (solid line) and fanning (dashed line) reversal, as shown in Fig. 4. The theoretical estimation in the figure is numerically presented on the left (normalized theoretical $H_c$) and bottom (particle number) axes with black color. The foothold of the estimation considers the total energy of the chain structure as follows:

$$E = -\frac{\mu^2}{a^3}(1 + \cos^2\theta) + 2\mu H \cos\theta, \quad (1)$$

where $\mu$ is the dipole magnetic moment, $a$ is the particle diameter, $\theta$ is the jointed angle between two dipole moments within two adjacent particles, and $H$ is the applied field. Each particle is treated as an $\mu$. The first term of the energy describes the mutual potential of the two dipoles, and the second term is associated with the potential energy of the chain in the presence of an external field. What makes coherent and fanning reversals different is $\theta$ in which the intrinsic $H_c$ of the two mechanisms can be gained by setting the second derivative of the energy to zero. Further details regarding model settings can be found in Ref. 24. For the purpose of clarity, we adopted reduced intrinsic (RI) $H_c$,[29] instead of intrinsic $H_c$, to eliminate the possibility of variations in moment from particle to particle.[19] We set the RI $H_c$ of coherent reversal to 1 as the theoretically maximum attainable $H_c$, to enable a better comparison with fanning reversal. In a similar fashion, we treated our experimental data to gain the RI $H_c$ of the five $Co_xNi_{1-x}$ samples.[29] The gained results were superimposed into Fig. 4, represented by upper (sample label) and right (normalized experimental $H_c$) axes using blue color. Surprisingly, when theoretical and experimental approaches are superimposed, the FCC group appears to lay in the fanning reversal region, while the HCP group is better described by coherent reversal. The excellent agreement between experimental data and the COS estimation unambiguously points out the structural geometry of the arrays as a factor of greater importance than $L_z$ in determining the coercive responses. It also suggests that the HCP arrays are likely to possess a strong interfacial exchange interaction[19] between particles, making coherent reversal more favorable than fanning. The discontinuity of $H_c$ is therefore ascribed to different mechanisms of the moment reversal, instead of the promoted orbital-lattice coupling through phase transition. We therefore conclude that changes in the magnetization of the $Co_xNi_{1-x}$ arrays are driven by itinerant Co-Ni $3d$ electronic exchange interactions; however, the coercive responses are governed by reversal dynamics confined by the framework of the arrays.

Figures 5(a) and 5(b) present the raw FORC measurements of CN50 and CN90 as representatives for the FCC and

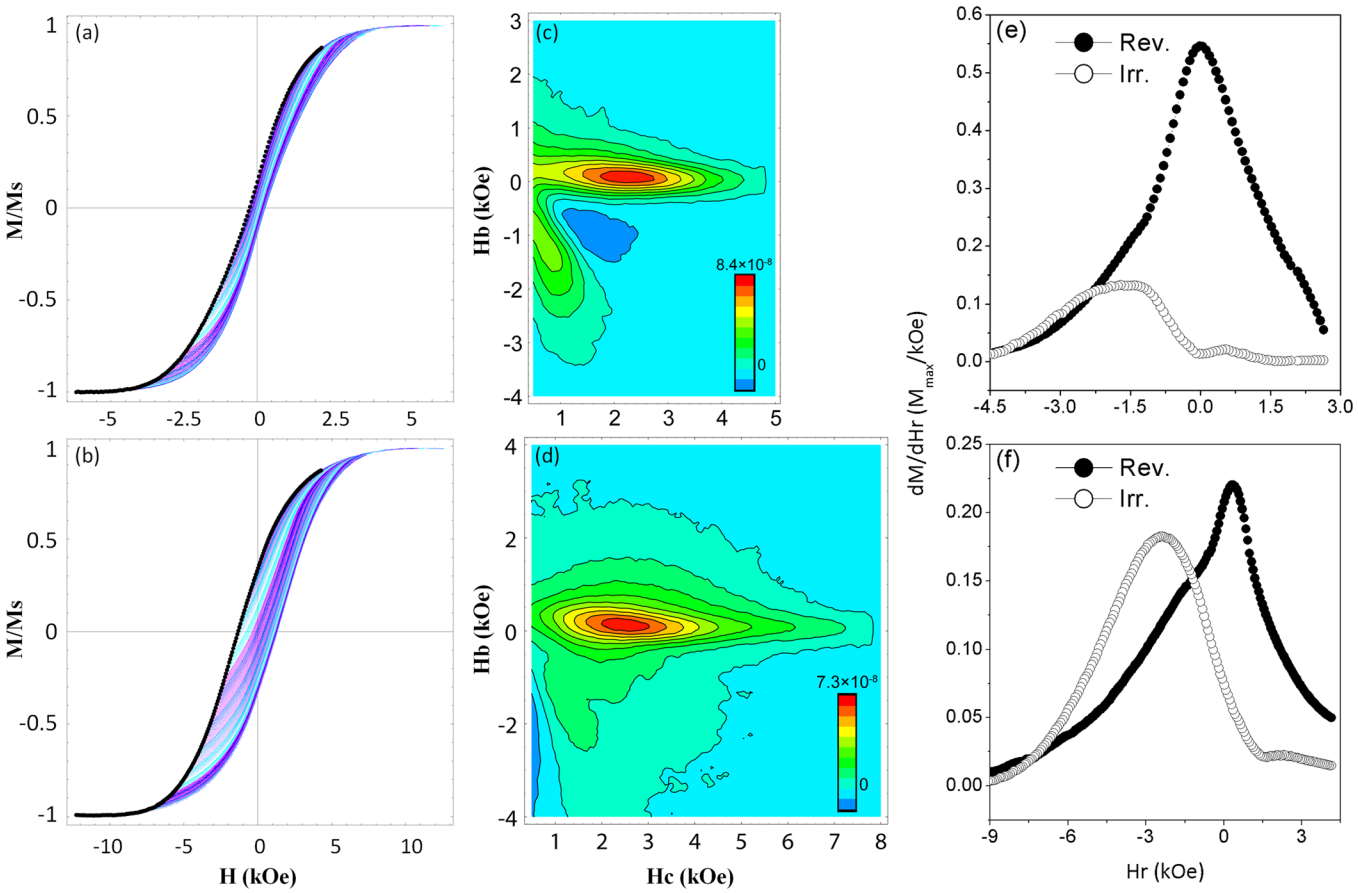


FIG. 5. Raw FORC measurements of (a) CN50 and (b) CN90, which represent the FCC and HCP arrays, respectively. (c) and (d) are the converted FORC contours, which correspond to (a) and (b), respectively. (e) Extracted reversible (filled-circles) and irreversible (open-circles) distributions of (e) CN50 and (f) CN90, which represent the FCC and HCP arrays, respectively. Data are calculated from the raw FORC measurements in Figs. 5(a) and 5(b).

HCP arrays, respectively. Figures 5(c) and 5(d) are the converted FORC contour diagrams corresponding to Figs. 5(a) and 5(b), respectively. In Fig. 5(c), the diagram presents a two-peak, bridge-like distribution, suggesting two major reversal components coexisting in the FCC arrays. One is located at the low $H_c$ and negative $H_b$ region, which can be thought of as a soft ferromagnetic component (SFM). The other extends along $H_c$ with the center located at an $H_c$ of ~2000 Oe, which can be thought of as a hard ferromagnetic component (HFM). In general, a soft component would generally generate a FORC distribution parallel to $H_b$; however, the variation in cluster size (Fig. 1(c)) may have modified the magnitude of the interaction field, causing a deviation in the distribution.[12] This distribution suggests that the FCC arrays tends to switch the SFM component in the beginning of the reversal, and subsequently complete the reversal by reversing the HFM component to reach the final state. In Fig. 5(d), the distribution of the HCP extends along $H_c$, suggesting the existence of a number of ferromagnetic components with different $H_c$s involved in the reversal process. The distribution center is located at $H_c$ ~2500 Oe, indicating the major contribution of an HFM component. The distribution also appears to broaden along $H_b$, suggesting the presence of a minor SFM. Considering that $H_b$ is related to the dipolar interactions, such broadening could be attributed to a strong interaction field between particles related to the strong magnetization of CN90. We further extracted reversible and irreversible components of CN50 and CN90 from their FORC diagrams, as shown in Figs. 5(e) and 5(f), respectively, using the methods described in Ref. 30. The decomposition of reversible and irreversible components is operated near the descending branch of the major loop by monitoring changes in magnetization versus $H_r$ changes in the original FORC (Figs. 5(a) and 5(b)); i.e., $dM/dH_r$. Further details can be found in Ref. 30. In Figure 5(e), a large reversible distribution coupled with the suppressed irreversibility was observed in the FCC arrays, similar to that obtained in Ni nanopillars.[12] Conversely, the HCP arrays display comparable reversible and irreversible contributions, indicating that the reversal may be coupled with a considerable irreversible path. FORC data provide insights into the reversal dynamics of the two groups beyond magnetization and coercivity. Coherency in the magnetization of the HCP arrays appears to arise from the interaction anisotropy among clusters, such that the arrays can be characterized as Stoner-Wohlfarth particles.[31,32] Therefore, the singly distributed, widely spread FORC diagram can be interpreted as the reversal overcoming the strong interaction anisotropy, comparable to what occurs in HCP-Co nanowires with a strong MCA effect[33] along the short axis of the wires featuring a similar FORC distribution.

In summary, this study investigated the correlation between the structural and magnetic properties of patterned $Co_xNi_{1-x}$ nano-arrays, focusing on the effects of structural geometry and microstructure. By isolating the magnetisms of Co and Ni using XMCD, the increase in the magnetization of $Co_xNi_{1-x}$ appears to stem from strong Co-Ni 3*d* exchange interactions. This was not expected according to Slater-Pauling theory in which magnetization is simply proportional to the sum of MV. Unlike other nanostructures, the MCA and coercivity effects of which are often $L_z$-driven, the sharply promoted $H_c$ through the FCC→HCP transition for $x \geqq 0.7$ can be attributed to the change in the moment reversal mechanism, resulting from the geometrical confinement and microstructural properties of the arrays. The two types of arrays were further probed using FORC technique to explore their reversal dynamics and reversibility. The FCC and HCP arrays both contained SFM and HFM. The greater intensity in the SFM of the FCC led to more pronounced reversibility than that observed with HCP.

The author would like to thank Mr. Fan-Hsiu Chang for the XMCD data collection at NSRRC beamline 11A. This work was supported by the National Science Council of Taiwan, under Grant No. NSC 101-2112-M-009 008-MY3.

[1]M. T. Rahman, R. K. Dumas, N. Eibagi, N. N. Shams, Y. C. Wu, K. Liu, and C. H. Lai, Appl. Phys. Lett. **94**, 042507 (2009).
[2]L. W. Wang, Y. C. Wu, and C. H. Lai, J. Appl. Phys. **105**, 07A713 (2009).
[3]Y. C. Wu, L. W. Wang, and C. H. Lai, Appl. Phys. Lett. **93**, 242501 (2008).
[4]C. Y. Yang, C. C. Huang, Y. C. Tseng, C. M. Liu, C. Chen, and H. J. Lin, J. Appl. Phys. **110**, 073913 (2011).
[5]Y. Inaba, T. Shimatsu, T. Oikawa, H. Sato, H. Aoi, and H. Muraoka, IEEE Trans. Magn. **40**, 2486 (2004).
[6]S. N. Piramanayagam, J. Appl. Phys. **102**, 011301 (2007).
[7]Y. Liu, T. A. George, R. Skomski, and D. J. Sellmyer, J. Appl. Phys. **111**, 07B537 (2012).
[8]D. Makarov, E. Bermúdez-Ureña, O. G. Schmidt, F. Liscio, M. Maret, C. Brombacher, S. Schulze, M. Hietschold, and M. Albrecht, Appl. Phys. Lett. **93**, 153112 (2008).
[9]M. Ohtake, S. Ouchi, F. Kirino, and M. Futamoto, J. Appl. Phys. **111**, 07A708 (2012).
[10]C. C. Huang, C. C. Lo, Y. C. Tseng, C. M. Liu, and C. Chen, J. Appl. Phys. **109**, 113905 (2011).
[11]C. T. Chen, Y. U. Idzerda, H. J. Lin, N. V. Smith, G. Meigs, E. Chaban, G. H. Ho, E. Pellegrin, and F. Sette, Phys. Rev. Lett. **75**, 152 (1995).
[12]C. R. Pike, C. A. Ross, R. T. Scalettar, and G. Zimanyi, Rhys. Rev. B **71**, 134407 (2005).
[13]R. K. Dumas, C. P. Li, I. V. Roshchin, I. K. Schuller, and K. Liu, Phys. Rev. B **75**, 134405 (2007).
[14]R. K. Dumas, K. Liu, C. P. Li, I. V. Roshchin, and I. K. Schuller, Appl. Phys. Lett. **91**, 202501 (2007).
[15]J. R. Davis, *Nickel, Cobalt, and Their Alloys* (ASM International, 2000), p. 358.
[16]A. R. Williams, V. L. Moruzzi, A. P. Malozemoff, and K. Terakura, IEEE Trans. Magn. **19**, 1983 (1983).
[17]A. Cebollada, J. M. García Martín, C. Clavero, Ll. Balcells, S. Estradé, J. Arbiol, F. Peiró, C. Smith, R. Clarke, L. Martínez, Y. Huttel, E. Román, N. D. Telling, and G. van der Laan, Phys. Rev. B **79**, 014414 (2009).
[18]H. Niu, Q. Chen, H. Zhu, Y. Lin, and X. Zhang, J. Mater. Chem. **13**, 1803 (2003).
[19]B. D. Cullity and C. D. Graham, *Introduction to Magnetic Materials* (John Wiley & Sons, Inc., Hoboken, New Jersey, 2009), pp. 364–368.
[20]J. Stöhr, J. Magn. Magn. Mater. **200**, 470 (1999).
[21]J. M. Shaw, H. T. Nembach, and T. J. Silva, Phys. Rev. B **87**, 054416 (2013).
[22]Y. C. Tseng, N. M. Souza-Neto, D. Haskel, M. Gich, C. Frontera, A. Roig, M. van Veenendaal, and J. Nogués, Phys. Rev. B **79**, 094404 (2009).
[23]C. Antoniak, J. Lindner, M. Spasova, D. Sudfeld, M. Acet, M. Farle, K. Fauth, U. Wiedwald, H.-G. Boyen, P. Ziemann, F. Wilhelm, A. Rogalev, and S. Sun, Phys. Rev. Lett. **97**, 117201 (2006).
[24]I. S. Jacobs and C. P. Bean, Phys. Rev. **100**, 1060 (1955).
[25]M. A. M. Haast, I. R. Heskamp, L. Abelmann, J. C. Lodder, and Th. J. A. Popma, J. Magn. Magn. Mater. **193**, 511 (1999).
[26]C. Luna, M. P. Morales, C. J. Serna, and M. Vázquez, Nanotechnology **14**, 268 (2003).
[27]P. Toneguzzo and O. Acher, IEEE Trans. Magn. **35**, 3469 (1999).
[28]H. Wu, P. Cao, W. Li, N. Ni, L. Zhu, and X. Zhang, J. Alloy. Compd. **509**, 1261 (2011).

[29]We followed the equation of RI $H_c = H_c/2\pi M_s$ from Ref. 19 to obtain reduced intrinsic $H_c$ (RI $H_c$). For CN70 and CN90, their intrinsic $H_c$ are $6.12*10^5$ and $5.54*10^5$ Oe/emu, respectively, which are greater than those of CN50 ($1.87*10^5$ Oe/emu), CN30 ($2.47*10^5$ Oe/emu), and CN10 ($2.17*10^5$ Oe/emu). This indicates that they belong to different groups. For a better comparison with the theoretical estimation in Fig. 7, we took the average of the RI $H_c$ of CN70 and CN90 and set it to be 1, and proportionally reduced RI $H_c$ of CN50, CN30, and CN10. Note that the information about the RI $H_c$ is presented by the ratio of coherent/fanning in this work, instead of absolute values of the two individuals, for the purpose of avoiding possible artifacts raised by $M_s$ normalization, cluster volume, or magnetic interactions among arrays etc., as well as having a clear comparison with the theory.
[30]M. Winklhofer, R. K. Dumas, and K. Liu, J. Appl. Phys. **103**, 07C518 (2008).
[31]C. Tannous and J. Gieraltowski, Eur. J. Phys. **29**, 475 (2008).
[32]J. Gong, S. Yang, C. Han, W. Guan, Y. Wang, B. Gao, D. Wang, X. Song, Z. Sun, and M. Xu, J. Appl. Phys. **111**, 063912 (2012).
[33]K. R. Pirota, F. Béron, D. Zanchet, T. C. R. Rocha, D. Navas, J. Torrejón, M. Vazquez, and M. Knobel, J. Appl. Phys. **109**, 083919 (2011).